American Mineralogist, Volume 75, pages 276–288, 1990

Interpreting one-dimensional high-resolution transmission electron micrographs of sheet silicates by computer simulation

GEORGE D. GUTHRIE, JR.,* DAVID R. VEBLEN
Department of Earth and Planetary Sciences, The Johns Hopkins University, Baltimore, Maryland 21218, U.S.A.

ABSTRACT

The computer-image simulation technique was used to address the interpretation of one-dimensional high-resolution transmission electron microscopy (1-D HRTEM) images of sheet silicates and their intergrowths. Simulated images as functions of focus and small variations in specimen orientation were calculated for kaolinite, lizardite, chlorite, vermiculite, muscovite, and phlogopite and for intergrown illite/smectite, phlogopite/chlorite, lizardite/chlorite, and brucite/chlorite.

The simulations showed that compositional periodicities resulting from interlayer cation ordering and structural information pertaining to layer sequence and approximate layer thickness can be inferred from simple 1-D HRTEM images of the basal planes of sheet silicates. However, different specific imaging conditions were required to image compositional periodicities and structural information properly. Compositional periodicities were best reflected in overfocused images; structural information was conveyed accurately only in images obtained near the Scherzer focus.

The simulated images varied strongly with specimen orientation and microscope focus. They showed that, in many cases, ambiguities may be present in the interpretation of experimental 1-D HRTEM images. The ambiguities, however, can be eliminated by an appropriate choice of imaging conditions (specimen orientation and focus). In materials where it is difficult to control these parameters accurately, such as clays and other fine-grained specimens, intuitive interpretations of 1-D HRTEM images may be in error.

INTRODUCTION

High-resolution transmission electron microscopy (HRTEM) has proved to be one of the most effective methods for studying fine-scale intergrowths involving sheet silicates. Such intergrowths can form either during primary growth or during replacement reactions, and the electron microscope is capable of providing both structural and compositional high-resolution data on these processes by imaging these intergrowths and analyzing regions containing only tens of layers. Furthermore, HRTEM information on sheet silicates can be obtained relatively easily, inasmuch as images of the basal spacings require orientation of one axis only, and these spacings are easily within the resolution of many commonly available TEM instruments. These one-dimensional images are often simple; nevertheless, their rigorous interpretation must be supported by computer image simulation.

HRTEM studies of sheet silicate intergrowths abound. Guthrie and Veblen (1989a) and Veblen et al. (1990) discuss several studies involving mixed-layer illite/smectite. HRTEM has been used to elucidate the reactions responsible for the replacement of biotite by chlorite (e.g., Veblen and Ferry, 1983; Amouric et al., 1988; Eggleton and Banfield, 1985; Olives Baños, 1985; Olives Baños and Amouric, 1984; Yau et al., 1984), of chlorite by biotite (e.g., Maresch et al., 1985), and of biotite by vermiculite (e.g., Banfield and Eggleton, 1988; Ilton and Veblen, 1988). HRTEM has also been used to characterize the structural state, and hence to suggest the formation mechanisms, for chlorite (e.g., Amouric et al., 1988) and intergrowths of phlogopite and serpentine (e.g., Livi and Veblen, 1987). The above studies used HRTEM to obtain predominantly one-dimensional lattice fringe images of the basal spacings. Though these images are relatively simple, a thorough understanding of the factors that can affect HRTEM images is fundamental to any interpretation based on such data.

The appearance of an HRTEM image is a complex function, not only of the structure being imaged and its orientation, but also of the imaging conditions (e.g., lens aberrations and focus conditions), so computer simulation is required to confirm that an image has been interpreted correctly. By simulating images of a presumed structure and then visually comparing the simulated images to the experimental images, atomic-level detail commonly may be inferred from high-resolution micrographs. This procedure was verified initially using images of metal oxides with known structures (e.g., Allpress et al., 1972; O'Keefe, 1973) and has since been used to in-

* Present address: Mail Stop D-469, Los Alamos National Laboratory, Los Alamos, New Mexico 87545, U.S.A.

0003–004X/90/0304–0276$02.00

terpret images of a wide range of carbonate (Meike et al., 1988) and silicate structures (e.g., Iijima and Buseck, 1978; Amouric et al., 1981; Veblen and Buseck, 1980; Spinnler et al., 1984). Various methods can be used to calculate HRTEM images; Self and O'Keefe (1988) discuss several procedures.

The image simulation technique has been applied successfully to the interpretation of two-dimensional HRTEM (2-D HRTEM) images of various sheet silicates. Iijima and Buseck (1978) used simulated images to show that the stacking order in muscovite is accurately reflected by the relative positions of white spots in 2-D HRTEM images obtained from crystals oriented with [100] parallel to the electron beam. Amouric et al. (1981) used simulated images to show that 2-D HRTEM images of *1M* F-phlogopite and *1M* and $2M_1$ muscovite are highly sensitive to experimental operating conditions (focus and sample thickness). Furthermore, "structure images," or images for which variations in intensity are directly proportional to the electrical potential in the sample, are obtainable only at very specific focuses for *1M* micas and perhaps are not obtainable under any conditions for some other structures. Finally, unless focus is adjusted with extreme care, misleading information pertaining to layer thickness, layer stacking, and site occupancy can be inferred from a purely intuitive interpretation of 2-D HRTEM images of micas. Spinnler et al. (1984) used simulated images to demonstrate that the same effects occur when imaging chlorite. To obtain useful polytype information from 2-D HRTEM images of chlorite, microscope focus and specimen orientation must be controlled. Even so, solitary images of a specimen do allow an unambiguous determination of the polytype; however, as with the micas, incorrect layer thicknesses can be inferred if image contrast is interpreted too literally.

Despite the general recognition of the need for image simulation, interpretation of one-dimensional images of sheet silicates and sheet-silicate intergrowths has been mostly intuitive, based upon extrapolation from two-dimensional image simulations for selected sheet silicates (Iijima and Buseck, 1978; Amouric et al., 1981; Spinnler et al., 1984). Because these structures can be divided into simple modules (i.e., brucite-like sheets, 1:1 layers, and 2:1 layers), image interpretation generally has followed an unwritten guideline that assumes the microscope was focused appropriately: dark fringes measuring ~1 nm overlie 2:1 layers, dark fringes measuring ~0.7 nm overlie 1:1 layers, and dark fringes measuring ~0.5 nm overlie brucite-like sheets.

When obtaining a high-resolution image with the TEM, the microscope can be focused quite accurately by first focusing the objective lens so that minimum contrast is observed in the thin edge of the specimen and then weakening the objective lens strength until its object plane is below the specimen by a specific amount (see Spence, 1988, section 10.5). This focus condition is sometimes referred to as the Scherzer focus and is generally considered to be the optimum focus condition for high-resolution imaging. (Scherzer focus is the focus condition used to obtain the structure images referred to above.) For structures with large unit cells, however, a faster method for focusing the microscope involves adjusting the objective lens until the anticipated high-contrast image appears (see Spence, 1988, section 10.3). Hence, a "correct" image of the chlorite structure would show one thick dark fringe and one thin dark fringe every 1.4 nm.

Recent studies, however, have demonstrated the need for computer simulation even when interpreting images of simple structures. Guthrie and Veblen (1989a) used computer image simulation to show that compositional periodicities resulting from the ordering of cations and vacancies in the interlayers of illite and smectite can be imaged with 1-D HRTEM; however, the focus conditions required to enhance the superperiodicities in the image are very different from the focus conditions normally used in HRTEM imaging. Specifically, compositional periodicities associated with mixed layering are not readily visible in images taken with the microscope focused to the Scherzer focus but are readily visible in images taken with the microscope overfocused. Furthermore, incorrect apparent layer thicknesses and fringe displacement resulting from slight deviations in specimen orientation make direct correlations between image and structure difficult for illite/smectite.

Guthrie and Veblen (1989b) demonstrated similar effects for thinner crystals (~8-nm thickness) of illite/smectite and reported some initial results on other structures. They also verified the technique for illite/smectite by showing that the simulated images compare very well with experimentally derived images. The importance of these image simulations is underscored by their application in recent interpretations of 1-D HRTEM images of mixed-layer illite/smectite (e.g., Veblen et al., 1990; Ahn and Peacor, 1990; Ahn and Buseck, 1989).

In this study, we discuss the interpretation of one-dimensional images for a larger range of sheet silicate structures. We used the technique verified by Guthrie and Veblen (1989b) to simulate 1-D HRTEM images of lizardite, kaolinite, chlorite, vermiculite, muscovite, phlogopite, and a variety of mixed-layer structures based on intergrowths of these minerals. The simulations addressed the following questions: (1) Can simple 1-D HRTEM images be simulated adequately for various structures? (2) How do 1-D HRTEM images of sheet silicates vary with focus and specimen orientation? (3) What is the correspondence between the image and structure? (4) What types of information can 1-D HRTEM images provide? (5) What are the limitations of 1-D HRTEM images of sheet silicates?

In this paper, we present 1-D HRTEM images that were calculated for a specific microscope, the Philips 420T. Consequently, the details in the simulated images do not apply to images taken from all microscopes. They do serve, however, to illustrate the types of variations to be expected in images taken with microscopes with optical characteristics that differ from those of the Philips 420T.

Methods

The simulated images were calculated using the SHRLI computer programs, version 80F (O'Keefe et al., 1978; O'Keefe, 1984), modified as described by Guthrie and Veblen (1989a). Calculations were performed on a Micro-VAX-II computer, and printed images were photocopied to increase contrast, arranged on paper, and photographed with Kodak Technical Pan High-Contrast Film developed in D-19 to produce the maximum contrast.

To simulate one-dimensional images of the basal spacings, all structure factors, F_{hkl}, that did not satisfy the conditions $h = 0$ and $k = 0$ were omitted during the formulation of the phase grating; hence, these calculations simulate the effects of dynamical interaction among the $00l$ diffracted beams only. Therefore, these simulated images differ slightly from those presented in Guthrie and Veblen (1989a), for which dynamical interaction was allowed to occur with the $0kl$ beams as well.

Electron-microscope optical parameters characteristic of a Philips 420T were used (point-to-point resolution = 0.34 nm; spherical aberration coefficient = 2 mm; chromatic aberration coefficient = 2 mm; accelerating voltage = 120 keV); such parameters are typical for many modern TEM instruments of moderate resolution. Sample thickness was assumed to be 15 unit cells parallel to **a** or about 8 nm. The contrast parameter was fixed for all calculations; the brightness parameter was adjusted to obtain images that were "exposed" properly, while the contrast parameter was adjusted to simulate images recorded on a high-contrast film. Different values for the contrast parameter (e.g., values characteristic of a lower contrast film) were used for some simulations and produced images that contained a wider range of tones; however, the major features in the images were unaffected. High-contrast images are presented here because they reproduce better.

Input structures were derived using z coordinates from various published structures; since the calculations addressed only variations perpendicular to the layers, x and y coordinates were unnecessary. H atoms were not considered in the calculations, and interlayer water was not considered in the simulations of the smectite structure.

The z coordinates for the dioctahedral micas (including illite and collapsed smectite) were taken from Richardson and Richardson (1982); the z coordinates for expanded smectite were derived from the collapsed smectite structure by "pulling apart" the adjacent 2:1 layers so that the distance between octahedral sheets increased from 1.0 nm to 1.2 nm. The z coordinates for phlogopite were taken from Hazen and Burnham (1973) and those for lizardite from Mellini (1982). The z coordinates for chlorite were taken from Bailey and Brown (1962); Al was assumed to replace Si in one quarter of the tetrahedral sites, and Fe was assumed to replace Mg in one third of the octahedral sites in the brucite-like sheet, thereby giving a formula of $[Mg_3Si_3AlO_{10}(OH)_2 \cdot Mg_2Fe(OH)_6]$, where Fe is assumed to be trivalent for charge balance.

The z coordinates for kaolinite were taken from the lizardite structure (Mellini, 1982). Magnesium in the octahedral sheet was replaced through the substitution

$$3Mg \rightarrow 2Al + 1\square$$

where $\square$ represents a vacancy. Though the oxygen positions in kaolinite differ somewhat from those in lizardite, such slight variations should not affect the images significantly. Furthermore, by using the same structure for lizardite and kaolinite, the effects of compositional variation could be assessed independently of those from structural variation.

The z coordinates for vermiculite were derived from the chlorite structure. Al was assumed to replace Si in one quarter of the tetrahedral sites. In the brucite-like sheet, water and vacancies were assumed to replace hydroxyl groups, and Mg and vacancies were assumed to replace Mg and Fe through the substitutions

$$6OH \rightarrow 4\,H_2O + 2\square$$
$$2Mg + 1Fe \rightarrow 0.5Mg + 2.5\square$$

thereby giving a formula of $[Mg_3Si_3AlO_{10}(OH)_2 \cdot Mg_{0.5}(OH_2)_4]$. As was the case with kaolinite, the oxygen positions in the interlayer sheet of vermiculite differ from those in chlorite; however, the differences are slight compared to the compositional difference between the two minerals.

Since no published structure refinements for intergrowths of lizardite, brucite, chlorite, and phlogopite exist, these structures were constructed by using z coordinates derived from the Bailey and Brown (1962) chlorite structure and the Hazen and Burnham (1973) phlogopite structure. Real-space distances between planes of atoms parallel to (001) were calculated and used to construct the polysomatic modules needed to build the various intergrowths (see Table 1 and Fig. 1), similar to the procedure suggested by Thompson (1978).[1] Following the notation of Thompson (1978), the modules used in this study would be designated B_D, B_U, T_D, T_U, P_D, and P_U, representing brucite, talc, and phlogopite, down and up. In this scheme, for example, brucite, lizardite, talc, a phlogopite/chlorite intergrowth, and a lizardite/chlorite intergrowth would be represented by the following:

$$\text{brucite} = B_D + B_U$$
$$\text{lizardite} = B_D + T_U$$
$$\text{talc} = T_D + T_U$$

[1] Note: The calculation of images using the multislice technique of Cowley and Moodie (1957) requires the structure to be periodic, since the calculation is made at discrete positions in reciprocal space. Images of aperiodic structures can be simulated with this technique, however, by embedding the aperiodic structure in a periodic structure, as described by Veblen (1985). In the present calculations, the intergrowth structures were made periodic by repeating the structure along **c***. The addition of extra layers did not affect the details of that part of the image corresponding to the intergrowth structure.

Table 1. Spacings between atomic planes

Atomic plane*	Spacing in nanometers	
	B & B**	Average†
Mg(1,2)-O(1),OH(1)	0.1008	0.1081
O(1),OH(1)-Si(1)	0.1680	0.1651
Si(1)-O(2,3)	0.0574	0.0571
O(2,3)-OH(2,3)	0.2800	0.2779
		0.2718‡
OH(2,3)-Mg(3,4)	0.0938	0.0965
		0.1165‡
O(2,3)-K		0.1667

* Atomic sites are named following the scheme by Bailey and Brown (1962); K is the interlayer site in a mica.

** Spacings extracted from the Bailey and Brown (1962) ideal chlorite structure as described in the text.

† Average of spacings extracted from the following structures (see Guthrie, 1989): Mathieson (1958), vermiculite; Gruner (1934), vermiculite; Shirozu and Bailey (1966), vermiculite; Shirozu and Bailey (1962), chlorite; Hazen and Burnham (1973), phlogopite; Richardson and Richardson (1982), muscovite; Lee and Guggenheim (1981), pyrophyllite; Perdikatsis and Burzlaff (1981), talc; Mellini (1982), lizardite.

‡ Average of spacings for the vermiculite structure only.

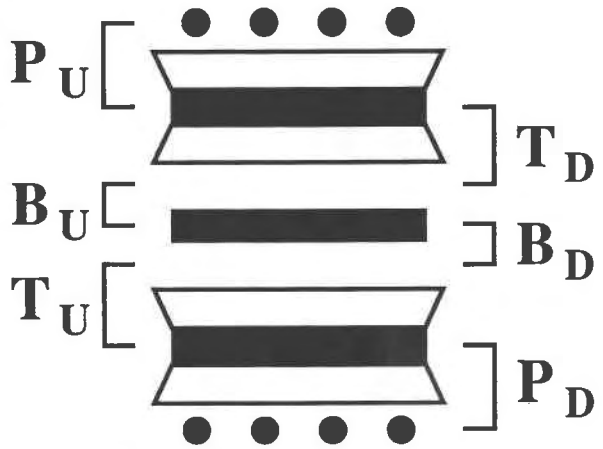

Fig. 1. Polysomatic modules used to construct the intergrowth structures. "B," "P," and "T" refer to brucite, phlogopite, and talc, and "D" and "U" refer to down and up, respectively.

$$\text{phlogopite/chlorite} = P_D + T_U + B_D + B_U + T_D + P_U$$

$$\text{lizardite/chlorite} = T_D + B_U + T_D + T_U + B_D + B_U$$

An independent test of this procedure is possible by comparing the calculated and observed $d_{(001)}$'s of brucite (calculated = 0.4676 nm; observed = 0.476 nm, Deer et al., 1966) and talc [calculated = 0.9324 nm; observed = (1.89 ÷ 2) nm, Deer et al., 1966]; the calculated and observed values differ by less than 2%. Such slight variations in atomic-interplanar spacings might affect the specifics of HRTEM images; however, the general interpretations presented here should be unaffected by these deviations. As an alternative method for calculating the spacings between the planes of atoms, spacings were averaged for various sheet silicate structures. Some images were calculated using these averaged parameters and showed no significant differences from the images calculated with the parameters derived from the Bailey and Brown (1962) and Hazen and Burnham (1973) structures (Table 1).

Observations

Simulated images were calculated for both simple-layer mineral structures and more complicated, mixed-layer intergrowth structures. The simple structures included kaolinite, lizardite, muscovite, phlogopite, chlorite, and vermiculite. The intergrowth structures included R1-illite/smectite (both with collapsed and with expanded smectite interlayers), phlogopite/chlorite, and various brucite/lizardite/chlorite intergrowths. A summary of results is given in Table 2.

Simple layer silicates

Kaolinite and lizardite. In the simulated 1-D HRTEM images of kaolinite, dark fringes approximately (but not exactly) overlay the 1:1 layers at some focus conditions, including the Scherzer focus, but reversals occurred within the focus range calculated (Fig. 2) such that dark fringes approximately (but not exactly) overlay the interlayers. Furthermore, the exact centers of these bright fringes varied by a few hundredths of a nanometer relative to the structure as focus changed. These variations are small and may not be obvious in the experimental images.

In general, the simulated images of lizardite very closely resembled those for kaolinite (Fig. 3). At Scherzer focus, dark fringes approximately overlay the 1:1 layers and light fringes overlay the interlayers. The reverse correspondence was true for overfocus.

Muscovite and phlogopite. The Scherzer-focused image of muscovite contained two bright fringes every 1.0 nm; thicker bright fringes overlay the interlayers (Fig. 4, $\Delta f = -100$ nm), and thinner bright fringes overlay the octa-

Table 2. Summary of results

Structure	Comments
0.7-nm (1:1) sheet silicates	Good portrayal of structure for $\Delta f = -125$ nm to -50 nm.
1.0-nm (2:1) sheet silicates	Accurate portrayal of structure for $\Delta f = -100$ nm (Scherzer focus); deviations of ±25 nm altered images significantly.
Vermiculite	Good portrayal of structure for $\Delta f = -100$ nm to -50 nm.
Chlorite	Good portrayal of structure for $\Delta f = -125$ nm to -100 nm; contrast reversal occurred at $\Delta f = -50$ nm.
R1-illite/smectite	Good portrayal of structure for $\Delta f = -100$ nm; good portrayal of compositional periodicity for $\Delta f > 0$ (exact focus differed for expanded and collapsed smectite). Some images contained misleading information.

Note: Values of focus apply exclusively to images taken under the following conditions: electron optics characteristic of the Philips 420T; **c*** normal to the electron beam (unless noted otherwise); specimen thickness of ~8 nm.

Fig. 2. Simulated 1-D HRTEM images of kaolinite shown as a function of focus conditions (shown beneath each image as deviations from Gaussian focus). Scherzer focus for the Philips 420T is approximately −100 nm. Simulations assumed the structure was oriented with the layers perfectly parallel to the electron beam.

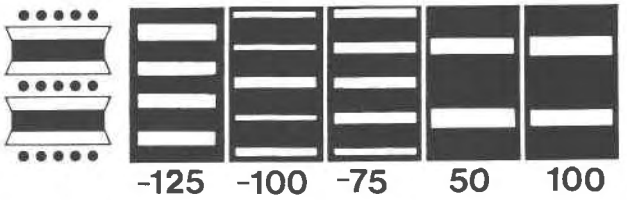

Fig. 4. Simulated 1-D HRTEM images of muscovite. Simulations assumed the structure was oriented with the layers perfectly parallel to the electron beam.

hedral sheets. Slight deviations from Scherzer focus rendered the two bright fringes indistinguishable, producing an apparent 0.5-nm periodicity ($\Delta f = -75$ nm); at overfocus conditions thick bright fringes were centered over the octahedral sheets only.

In the Scherzer-focused image of phlogopite, bright fringes overlay the interlayers (Fig. 5, $\Delta f = -100$ nm). However, reversals of the image occurred at a finer focus interval for phlogopite than for muscovite, such that bright fringes overlay the octahedral sheets at $\Delta f = -125$ nm and $\Delta f = -75$ nm. At the overfocus values calculated, bright fringes overlay the interlayers ($\Delta f = 50$ nm, 100 nm).

Chlorite and vermiculite. The true 1.4-nm periodicity of chlorite was clearly evident in the simulated images for most values of defocus (Fig. 6); however, at some values of defocus (e.g., $\Delta f = 0$ nm), an apparent 0.7-nm periodicity predominated. The Scherzer-focused image did resemble typical published one-dimensional images of chlorite with one thick dark fringe and one thin dark fringe per 1.4 nm; in these images, thick dark fringes overlay the 2:1 layers and thin dark fringes overlay the brucite-like sheets. However, this correspondence was a function of both the focus and specimen orientation conditions, and a reversal occurred near $\Delta f = -50$ nm such that thick dark fringes overlay the brucite-like layers and thin dark fringes overlay the 2:1 layers; thus, the image strongly resembled the image obtained at the Scherzer focus but was shifted by one half the unit cell translation parallel to **c***.

As with the images of chlorite, the images of vermiculite showed that the 1.4-nm periodicity can be imaged (Fig. 7). Over the range of defocus calculated for this structure (−100 nm to −50 nm, in steps of 10 nm), the vermiculite images could be distinguished from the chlorite images inasmuch as the vermiculite images contained only one dark fringe per 1.4 nm whereas the chlorite images contained two dark fringes per 1.4 nm. At the Scherzer focus, the simulated images of vermiculite showed dark fringes centered over the 2:1 layer and bright fringes centered over the interlayer region. Furthermore, no image reversal occurred between $\Delta f = -100$ nm and $\Delta f = -50$ nm, as it did for the chlorite images.

Intergrowth structures

R1-illite/smectite. Simulated 1-D HRTEM images of R1-illite/smectite with a collapsed smectite interlayer are shown in Figure 8. These simulations were calculated for a thinner specimen (~8 nm) than the images presented in Guthrie and Veblen (1989a). The general observations on the simulated images of the thinner specimen were the same as those for the thicker specimen. The compositional periodicity was weak in images taken at the Scherzer focus but was readily apparent in images taken at overfocus. In overfocused images, thick dark fringes overlay the smectite interlayers and thin dark fringes overlay the illite interlayers; the input structure for the simulations shown in Figure 8 assumed both interlayers to have the same thickness.

The substitution of Na for K in the interlayer produced only minor changes in the images (Fig. 9); however, the compositional periodicity was slightly more difficult to detect in the overfocused images, consistent with the smaller difference in potential between I and S interlayers that results from the lower atomic number of Na.

Simulated 1-D HRTEM images of R1-illite/smectite with the smectite interlayer expanded so that the distance between octahedral sheets increased from 1.0 nm to 1.2 nm

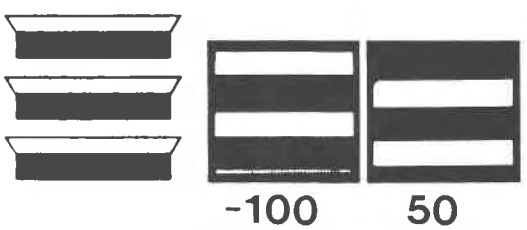

Fig. 3. Simulated 1-D HRTEM images of lizardite. Simulations assumed the structure was oriented with the layers perfectly parallel to the electron beam.

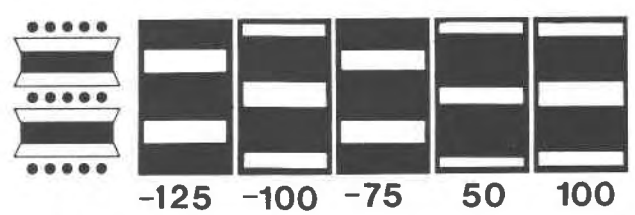

Fig. 5. Simulated 1-D HRTEM images of phlogopite. Simulations assumed the structure was oriented with the layers perfectly parallel to the electron beam.

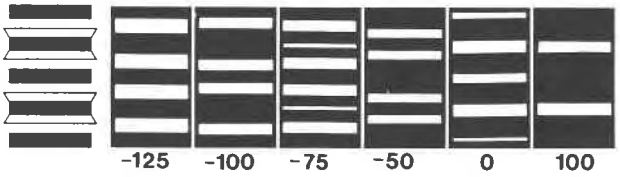

Fig. 6. Simulated 1-D HRTEM images of chlorite. Simulations assumed the structure was oriented with the layers perfectly parallel to the electron beam.

are shown in Figure 10. For the Scherzer-focused image, the 2-layer periodicity was present but not readily apparent ($\Delta f = -100$ nm); a 1-layer subperiodicity was indicated by thick bright fringes spaced at a uniform 1.1 nm, and the 2-layer periodicity was manifested by thinner bright fringes. In overfocused images, the 2-layer periodicity was readily apparent at $\Delta f = 50$ nm but not apparent at $\Delta f = 100$ nm. These images further differed from those of the R1-illite/smectite with the collapsed smectite interlayer, in that thick dark fringes overlay the illite interlayers and thin dark fringes overlay the smectite interlayers, giving the appearance of an expanded illite layer and a collapsed smectite layer.

Figure 11 shows simulated images for the same structure tilted approximately 2° so that the layers were no longer parallel to the electron beam. Two features distinguished the images of tilted, expanded R1-illite/smectite from the images of the nontilted structure. First, the positions of the fringes were displaced relative to the structure. Second, in overfocused images, thick dark fringes overlay the smectite interlayers and thin dark fringes overlay the illite interlayers; hence, the images of the tilted structure mimicked the overfocused images of the collapsed R1-illite/smectite.

Phlogopite/chlorite intergrowths. The Scherzer-focused image of intergrown phlogopite/chlorite accurately reflected the underlying structure (Fig. 12, $\Delta f = -100$ nm): thick dark fringes overlay the 2:1 layers and thin dark fringes overlay the brucite-like sheet. The image remained roughly the same for small deviations in focus; however, the thick dark fringes no longer exactly overlay the 2:1 layers but were displaced up to 0.2 nm relative to the structure (e.g., $\Delta f = -125$ nm). The 2.4-nm periodicity was apparent over the entire range of focus calculated ($\Delta f = -150$ to $\Delta f = 100$ nm, shown is $\Delta f = -125$ nm to $\Delta f = 50$ nm).

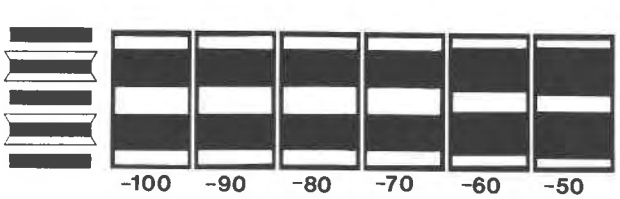

Fig. 7. Simulated 1-D HRTEM images of vermiculite. Simulations assumed the structure was oriented with the layers perfectly parallel to the electron beam.

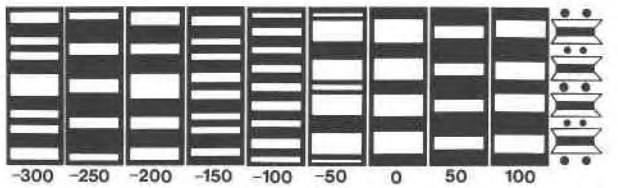

Fig. 8. Simulated 1-D HRTEM images of an R1-illite/smectite with collapsed smectite interlayers. Simulations assumed that K was the only interlayer cation and that the structure was oriented with the layers perfectly parallel to the electron beam.

Brucite/lizardite/chlorite intergrowths. Figure 13 shows simulated 1-D HRTEM images of two lizardite layers intergrown with chlorite in the following sequence: brucite-talc-lizardite-brucite-lizardite-talc (BTLBLT). The Scherzer-focused image accurately reflected the underlying structure, and individual layers were recognized ($\Delta f = -100$ nm). Thick dark fringes overlay talc layers, slightly thinner dark fringes overlay lizardite layers, and the thinnest dark fringes overlay the brucite-like sheet. Slight deviations in focus (as little as ± 25 nm) degraded the image so that the unit-cell periodicity was retained, but individual layers could not be recognized.

Figure 14 shows simulated HRTEM images for the same structure (BTLBLT) tilted approximately 2°. Tilting the structure degraded the image slightly and shifted the fringes relative to the structure; however, individual layers were still recognized at the Scherzer focus.

Simulated 1-D HRTEM images were calculated for several other intergrowth structures, including the following: BTBLLT, BTLBBT, BTBLT, BTBBT, BTBBBT, and BTBBBBT. The general observations that applied to the images of the structure BTLBLT also applied to the images of these structures. The structures were accurately portrayed in Scherzer-focused images. Slight deviations in focus, however, degraded the images and led to possible ambiguous images that in all likelihood would be misinterpreted.

Discussion

The simulated images presented above showed that important structural and chemical information can be de-

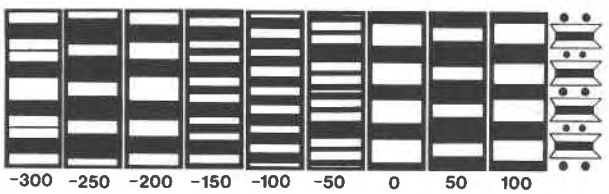

Fig. 9. Simulated 1-D HRTEM images of an R1-illite/smectite with collapsed smectite interlayers. Simulations assumed that Na was the only interlayer cation and that the structure was oriented with the layers perfectly parallel to the electron beam.

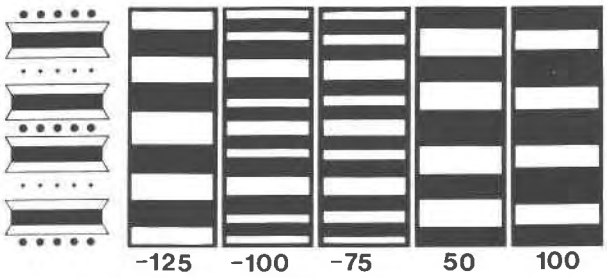

Fig. 10. Simulated 1-D HRTEM images of an R1-illite/smectite with smectite interlayers expanded from 1.0 nm to 1.2 nm. Simulations assumed that K was the only interlayer cation and that the structure was oriented with the layers perfectly parallel to the electron beam.

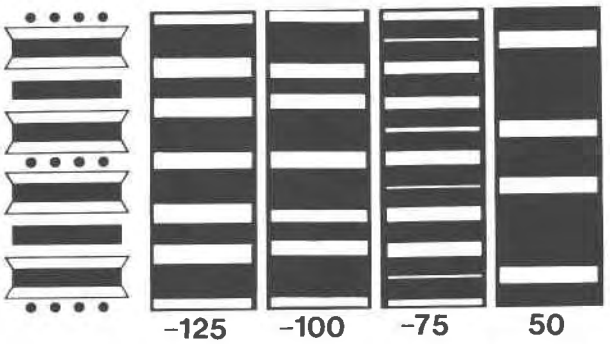

Fig. 12. Simulated 1-D HRTEM images of a phlogopite/chlorite intergrowth. Simulations assumed the structure was oriented with the layers perfectly parallel to the electron beam.

rived from 1-D HRTEM images of sheet silicates. The imaging conditions (focus, specimen orientation) strongly affected the images, and different imaging conditions were required to reveal compositional periodicities effectively (i.e., one-dimensional cation ordering) versus structural information (i.e., layer sequence). In general, compositional periodicities were absent or very difficult to observe in Scherzer-focused images, but they were readily apparent in overfocused images. Layer sequences, however, were portrayed accurately only in Scherzer-focused images. Slight deviations in focus degraded the images so that such structural information could only be obtained by comparing the computer-simulated image to the input structure; hence, experimental images taken with the microscope focused similarly must be interpreted by comparing them to the simulated images. Furthermore, several ambiguities in interpretation were illustrated by the simulations.

Correspondence between image and structure

Effect of focus. The simulated images showed contrast reversals for all structures within the focus range $\Delta f = -150$ nm to 100 nm. In Scherzer-focused images, bright fringes commonly overlay regions of relatively low charge density, and dark fringes overlay regions of high charge density. However, this was not always true, as the bright fringes in some cases were not centered over the regions of low electron density, and therefore they also overlay regions of higher charge density. For example, the positions of the bright fringes in the kaolinite and lizardite structures were displaced relative to the centers of the interlayer regions. Also, the thinner bright fringes in the simulated images of expanded R1-illite/smectite did not overlay the octahedral sheets directly but were displaced slightly to one side, whereas the corresponding bright fringes in the simulated images of collapsed R1-illite/smectite directly overlay the octahedral sheets.

Even slight deviations from Scherzer focus altered the following relationship: bright fringe = low charge density, dark fringe = high charge density. Very slight deviations in focus resulted in slight displacements of the bright fringes into positions not directly overlying the regions of low charge density. Larger deviations resulted in complete contrast reversals, so that bright fringes overlay regions of high charge density. For some structures the reversals occurred for small deviations from Scherzer focus (e.g., the phlogopite structure, Fig. 5); other structures maintained a "normal" correspondence for large deviations from Scherzer focus (e.g., the kaolinite structure, Fig. 2).

Contrast reversal is problematical because it is not always possible to determine from the image if contrast is normal or reversed. In addition, it is not always possible in experiments with sheet silicates for the miroscopist to set the focus to better than ± 25 nm, due to rapid beam damage and other constraints. For the structures based on one structural unit (e.g., only 1:1 layers or only evenly spaced 2:1 layers), reversed images typically were indistinguishable from normal images; hence, in experimental images, it is impossible to determine whether a bright fringe corresponds to a region of low charge density without knowing the exact focus value. For chlorite, some "reversed" images were distinguishable from the normal image at Scherzer focus (e.g., compare Fig. 6, $\Delta f = -100$ nm and $\Delta f = 100$ nm); however, other reversed images strongly resembled the Scherzer-focused image (e.g., compare Fig. 6, $\Delta f = -100$ nm and $\Delta f = -50$ nm). Thus,

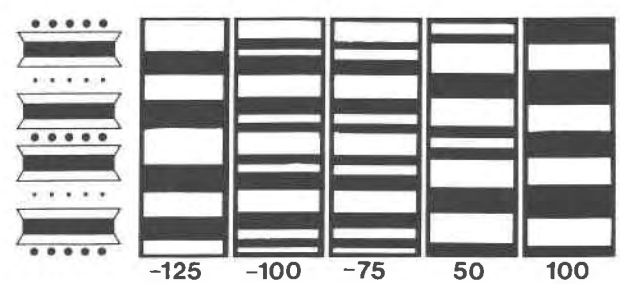

Fig. 11. Simulated 1-D HRTEM images of an R1-illite/smectite with smectite interlayers expanded from 1.0 nm to 1.2 nm. Simulations assumed that K was the only interlayer cation and that the structure was oriented with the layers tilted approximately 2° relative to the electron beam.

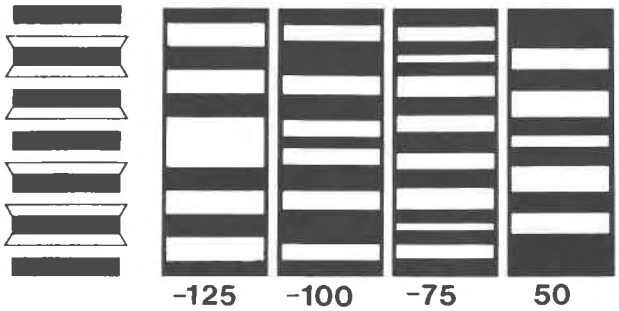

Fig. 13. Simulated 1-D HRTEM images of an intergrowth of chlorite and lizardite forming the sequence BTLBLT. B, T, and L refer to brucite, talc, and lizardite, respectively. Simulations assumed the structure was oriented with the layers perfectly parallel to the electron beam.

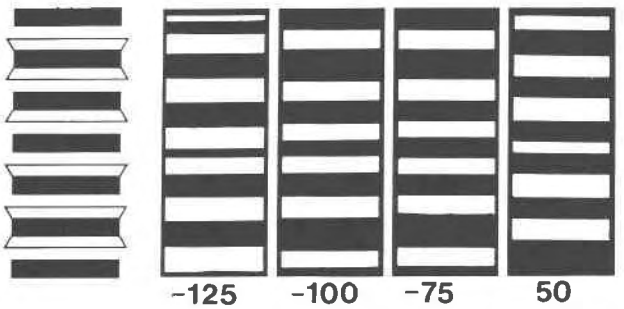

Fig. 14. Simulated 1-D HRTEM images of an intergrowth of chlorite and lizardite forming the sequence BTLBLT. Simulations assumed the structure was oriented with the layers tilted approximately 2° relative to the electron beam.

even in structures based on more than one structural unit (e.g., combinations of 2:1 layers, 1:1 layers, brucite-like sheets, and interlayer cations), focus must be controlled carefully (or at least known) in order to determine whether a bright fringe corresponds to a region of low charge density in an experimental image.

Effect of specimen orientation. Tilting the silicate layers slightly with respect to the electron beam caused a loss in image detail and a displacement of the fringes relative to the structure. Over the tilt range calculated (0° to approximately 3°), the amount of displacement was a function of the input structure, focus, and the amount of tilt away from perfect orientation. Guthrie and Veblen (1989a) discussed the effect of specimen orientation in greater detail with respect to R1-illite/smectite. In the present study, the layer sequence was represented accurately in images of structures tilted up to about 2°, though the fringes were displaced relative to layers of the structure.

Electron optical illusions

Subperiodicities. Simulated images for R1-illite/smectite (both collapsed and expanded) and chlorite both contained dominant subperiodicities for some values of focus. Scherzer-focused images of the collapsed R1-illite/smectite showed a dominant 1.0-nm periodicity; Scherzer-focused images of the expanded R1-illite/smectite showed a dominant 1.1-nm periodicity. Images of chlorite showed a dominant 0.7-nm periodicity at $\Delta f = 0$ nm.

The presence of dominant subperiodicities in collapsed R1-illite/smectite was discussed by Guthrie and Veblen (1989a). It was noted that the absence of a superperiodicity in a 1-D HRTEM image of illite/smectite does not necessarily mean that compositional ordering is not present in the specimen. In addition to verifying the observations for thinner specimens, the calculations presented here showed that this same caution should be applied even if the smectite layers may have remained expanded in the vacuum of the electron microscope.

It has been shown that chlorite can grow upon heating from a 0.7-nm 1:1 precursor phase (e.g., Nelson and Roy, 1958), and some HRTEM studies of diagenetically altered sediments have documented this process in natural materials (e.g., Amouric et al., 1988; Ahn and Peacor, 1985). However, the simulations demonstrated that 1-D HRTEM images of chlorite can appear to contain a 0.7-nm repeat for some values of defocus (e.g., Fig. 6, $\Delta f = -125$ nm and $\Delta f = 0$ nm). In fact, all simulated images in the $\Delta f = -125$ nm to $\Delta f = -140$ nm contained a predominant 0.7-nm periodicity; this effect was even more profound when an objective aperture excluding information ≤ 0.5 nm was used. (An objective aperture corresponding to the point-to-point resolution of the Philips 420T, 0.34 nm, was used in the simulations presented in this paper.) Therefore, the same cautions suggested for the interpretation of images of illite/smectite apply to the interpretation of images of chlorite. The presence of a 0.7-nm periodicity in an 1-D HRTEM image does not prove the presence of a 0.7-nm phase, unless images taken at more than one focus are compared or it is clear that appropriate underfocused conditions were used for the experiment.

Layer thickness. Guthrie and Veblen (1989a) demonstrated that incorrect layer thicknesses could be deduced by an intuitive interpretation of one-dimensional images of R1-illite/smectite. Specifically, smectite layers appear to be expanded in overfocused images despite the smectite layers being fully collapsed in the specimen. Spinnler et al. (1984) reported a similar finding in two-dimensional simulated images of chlorite. The simulations presented here clearly demonstrate that the effect is not restricted to two-dimensional images of chlorite or images of collapsed R1-illite/smectite.

The simulated images of the expanded R1-illite/smectite showed an incorrect apparent periodicity ($\sim$1.1 nm) for some defocus values (e.g., Fig. 10, $\Delta f = -125$ nm, -75 nm). At such defocus values, individual layers appeared to be the same thickness when measurements were made between centers of the thick bright fringes. In fact, this observation correctly reflects the underlying structure, since the thick bright fringes corresponded to the interlayer sites, and the interlayer sites were evenly spaced at 1.1 nm. Because the bright fringes were the dominant

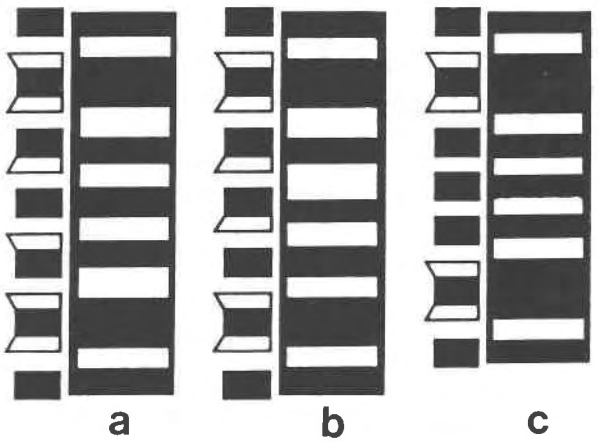

Fig. 15. Comparison of images of various intergrowth structures. Simulations assumed the structures were oriented with the layers perfectly parallel to the electron beam. (**a**) BTLBLT; $\Delta f = -75$ nm. (**b**) BTBLLT; $\Delta f = -75$ nm. (**c**) BTBBBT; $\Delta f = -100$ nm.

feature, the image appeared to contain layers of equal thickness. To determine layer thicknesses of illite/smectite correctly, measurements must be made between the centers of the octahedral sheets; in the structure with the expanded smectite interlayer, the octahedral sheets were spaced at 1.0 nm and 1.2 nm. At Scherzer focus, however, no fringes directly overlay the octahedral sheets, so only an approximate measurement could be made. Furthermore, overfocused images of the perfectly oriented structure (Fig. 10, $\Delta f = 100$ nm) incorrectly implied an expanded illite layer and a collapsed smectite layer. The images of the tilted structure, however, showed the reverse; thick dark fringes overlay the smectite layer and thin dark fringes overlay the illite layer (Fig. 11, $\Delta f = 100$ nm).

Another example of apparently incorrect layer thickness occurred in the simulated images of the brucite-lizardite-chlorite intergrowth structures.Though the Scherzer-focused images accurately portrayed the relative thicknesses of the brucite sheets, 1:1 layers, and 2:1 layers, slight deviations in focus rendered the brucite sheets indistinguishable from the 1:1 layers (Figs. 13 and 14, $\Delta f = -75$ nm). Thus, structures with differing sequences (e.g., BTLBLT and BTBLLT) could not be discriminated (Fig. 15). Furthermore, those structures could not be discriminated from the structure BTBBBT by a visual estimation of the differences between individual layers. However, they could be distinguished by careful measurement of the total repeat between thick dark fringes (i.e., 2:1 layers).

Determination of average fringe thickness. In practice, ambiguities can be eliminated in some cases by a determination of the average fringe thickness within a region. If the total thickness of a unit and the number of fringes in the unit are known, then an average fringe thickness can be determined, and some proposed structures can be eliminated. A measurement can be made across several fringes and normalized to the total number measured, as is commonly done when measuring electron micrographs; however, the measurement actually desired, as opposed to the measurement being made, should be carefully considered so that an accurate average fringe thickness is determined. In other words, if extra layers are included in the measurement, their thickness should be taken into consideration.

For example, a determination of the average fringe thickness for the structures LBL (or BLL) and BBB would allow the above sequences (BTLBLT, BTBLLT, and BTBBBT) to be distinguished. Measurements between thick dark fringes (2:1 layers) in an experimental image would enable the average fringe thickness to be determined. However, such a measurement would include the equivalent of one talc layer's thickness, since the sequences are bounded by one T_U layer and one T_D layer. The width of one talc layer (0.9324 nm, calculated from the Bailey and Brown model as described above) must be subtracted from the initial sequence-measurements (TLBLT = 2.8 nm; TBBBT = 2.3352 nm) so that an accurate average fringe thickness can be determined. The average fringe thickness clearly distinguishes the two sequences, since the average fringe thickness for the sequence LBL is 0.6225 nm, whereas the average fringe thickness for the sequence BBB is 0.4676 nm. When large numbers of fringes are present in a sequence, however, minor differences may be indistinguishable in experimental images, since measurement errors from HRTEM images are generally about 5% (Spence, 1988).

Previous interpretations

Numerous studies have presented conclusions based in part on interpretations of 1-D HRTEM images of sheet silicates that should be reexamined in light of the simulations presented in this paper and in Guthrie and Veblen (1989a, 1989b).

Lizardite and kaolinite. In the simulated images of lizardite and kaolinite, a 0.7-nm periodicity was visible over the entire range of focus calculated ($\Delta f = -150$ nm to 100 nm), and a dark fringe approximately overlay the 1:1 layer for underfocus conditions. Since underfocus conditions are normally used in HRTEM imaging, the dark fringes in most published experimental images of lizardite and kaolinite probably lie very close to the 1:1 layers (e.g., Amouric et al., 1988; Livi and Veblen, 1987; Ahn and Peacor, 1987a, 1987b; Lee et al., 1986b; Veblen, 1983; Veblen and Buseck, 1979). However, tilting shifts the image relative to the structure, so exact correlation between fringe position and structural layers is possible only for images obtained from specimens that were oriented with their layers precisely parallel to the electron beam. Furthermore, since chlorite can show an apparent 0.7-nm periodicity at some focuses, some images previously assumed to contain a 0.7-nm phase may represent chlorite, rather than a 1:1 silicate. Indeed, some published images show subtle signs of a 1.4-nm periodicity (e.g., Yau et al.,

1984, Figs. 3c, 3d). These images may represent a chlorite-like phase or a two-layer polytype of a 0.7-nm layer phase, but it is not possible to tell which without additional information such as electron diffraction patterns or through-focus series.

Phlogopite and muscovite. Structural correlation for 1-D HRTEM studies of biotite and muscovite is more difficult. Reversals in image contrast occurred with small changes in focus for the simulated images of phlogopite, making structural correlation for published images of biotite impossible, since the exact defocus cannot be determined from an experimental image containing only biotite; one must therefore assume that the microscopist recorded the image at optimum defocus if one wishes to make such correlations. Detailed structural interpretations of images of pure biotite are not usually necessary, but they are more commonly required of images representing intergrowths of biotite with other phases. When biotite is intergrown with another phase, it may be possible to use simulated images to estimate the defocus from published images and thereby provide a means of correlating fringes to a structure, since the simulated images of intergrowth structures indicate that such experimental images are highly sensitive to focus. The simulated images of muscovite were less sensitive to changes in focus than those for biotite, and thick bright fringes overlay the interlayers for the underfocus conditions calculated. Furthermore, at the Scherzer focus, thinner bright fringes overlay the octahedral sheets as well. Since thinner bright fringes were not present in the reversed-contrast images, the presence of these fringes appears to be indicative of Scherzer-focus conditions. In some cases these thinner bright fringes can be seen in experimental images (e.g., Veblen et al., 1990; Guthrie and Veblen, 1989b; Veblen, 1983), and structural correlation can be made easily. For images in which these fringes are not present, structural correlation is less certain.

Chlorite and vermiculite. Many published experimental images of chlorite strongly resemble our simulated images, showing one thick dark fringe and one thin dark fringe per 1.4 nm (e.g., Amouric et al., 1988; Lee et al., 1986a, Fig. 9b; Ahn and Peacor, 1985, Fig. 2; Lee et al., 1985, Fig. 8; Veblen, 1983). Unfortunately, because the structural correlation reverses between $\Delta f = -125$ nm and $\Delta f = -50$ nm, correlation between the image and structure is difficult for images of pure chlorite, so in order to make structural correlations, one must again assume that the microscopist used the correct focus condition. As with biotite, it may be possible to determine the exact focus condition when chlorite is intergrown with other phases, thereby enabling a better correlation between the image and structure.

Some published experimental images of chlorite do not resemble our simulations closely. Specifically, in some images the 1.4-nm periodicity appears as one thick light fringe and one thin light fringe per 1.4 nm (e.g., Lee and Peacor, 1985; Ahn and Peacor, 1985, Figs. 3 and 6; Ahn et al., 1988, Figs. 6–8) or one light fringe per 1.4 nm (e.g., Veblen and Ferry, 1983, Figs. 3 and 8). The lack of correlation between these images and our simulations is probably due to differences in orientation or thickness of the crystal, differences in focus, and differences in microscope optics for these studies compared to those used for our simulations. Alternatively, some of these images may contain phases other than chlorite.

The simulated images of vermiculite showed a 1.4-nm periodicity with the microscope focused to within 50 nm of the Scherzer focus. These images contained only one dark fringe per 1.4 nm, so the Scherzer-focused image did not contain a thin dark fringe over the interlayer sheet as did the Scherzer-focused image of chlorite. These features are consistent with some published images of vermiculite (Ilton and Veblen, 1988; Banfield and Eggleton, 1988, Fig. 8 and *some* of the fringes labeled "V" in Fig. 11). Hence, vermiculite and chlorite apparently can be distinguished in 1-D HRTEM images taken with the microscope focus near the Scherzer focus. However, since 1-D HRTEM images of chlorite at some focuses (e.g., Fig. 6, $\Delta f = 50$ nm) can resemble vermiculite, chlorite and vermiculite can be distinguished in 1-D HRTEM images only if the focus is controlled carefully. When focus cannot be carefully controlled (e.g., when the specimen damages too rapidly in the electron beam), compositional analyses from the region may help distinguish the two minerals. However, since chlorite is beam-damaged relatively slowly as compared to many other sheet silicates, careful control of focus should normally be possible.

The difference between chlorite and vermiculite in images taken at the Scherzer focus is a dark fringe overlaying the brucite-like sheet; this fringe is present in images of chlorite and absent in images of vermiculite. The presence (or absence) of this fringe, therefore, may be a measure of the amount of material occupying the interlayer region. The presence of both a thin dark fringe and a thick dark fringe per 1.4 nm in Scherzer-focused images suggests a high interlayer occupancy (chlorite-like), whereas the presence of only a thick dark fringe per 1.4 nm indicates a low interlayer occupancy (vermiculite-like). Some published 1-D HRTEM images of chlorite contain only one dark fringe per 1.4 nm (e.g., Veblen and Ferry, 1983, Figs. 3 and 8). The interlayer region in these images may be occupied by an incomplete brucite-like sheet. Furthermore, many published 1-D HRTEM images of vermiculite contain both a thick dark fringe and a thin dark fringe per 1.4 nm (e.g., Banfield and Eggleton, 1988, some fringes labeled "V" in Fig. 11). The interlayer regions that show a thin dark fringe in these images may have higher occupancies than the interlayer regions that do not show a thin dark fringe. The presence of vermiculite in the material presented by Banfield and Eggleton (1988) was verified with XRD. One explanation is that this sample may possess interlayers with three different occupancies or perhaps interlayers with a range of occupancies. The different interlayer occupancies appear as thin light fringes (a mica-like interlayer), thick light fringes (either a vermiculite-like or smectite-like interlayer), and thin dark

fringes bounded by thin light fringes (either a chlorite-like or vermiculite-like interlayer). Clearly, a detailed study of well-characterized samples using both experimental and computer-simulated HRTEM would clarify the discrepancies between the simulations and images.

Illite and smectite. Guthrie and Veblen (1989a) discussed in detail many problems associated with the interpretation of 1-D HRTEM images of cation ordering along c* in mixed-layer illite/smectite. We showed that images taken with the microscope in the standard focus condition for HRTEM (Scherzer focus) do not readily show the compositional periodicity; however, images taken with the microscope overfocused clearly show the periodicity. Hence, compositional periodicity may be unobserved in specimens where it is present, unless the proper overfocus conditions are used.

Several recent studies have used these results to observe the compositional periodicity in mixed-layer illite/smectite. Veblen et al. (1990) and Ahn and Peacor (1990) demonstrated that sequences of illite and smectite layers can be determined directly from images when appropriate imaging conditions are used. However, the ambiguous images of illite/smectite that can be obtained at the Scherzer focus and under many other conditions have necessitated the reinterpretation of some studies (i.e., Ahn and Peacor, 1989, 1986). Furthermore, since layer sequences can be misinterpreted even when the smectite interlayers have not fully collapsed (Fig. 10, $\Delta f = -100$ nm and $\Delta f = 50$ nm), some ambiguities can be eliminated only when other data are available (e.g., X-ray data or compositional data, as were used in Veblen et al., 1990).

Other intergrowth structures. It is clear from the simulations that ambiguous information can be present in 1-D HRTEM images if the focus is not controlled appropriately but that Scherzer-focused images from well-oriented crystals do contain accurate information pertaining to variations in layer thickness (though not necessarily absolute layer thickness). Many studies have successfully imaged individual layers of a different material intergrown with an otherwise defect-free host, such as intergrowths of 0.7-nm and 1.4-nm phases (e.g., Amouric et al., 1988; Ahn and Peacor, 1985) and 1.0-nm and 1.4-nm phases (Ahn et al., 1988; Veblen, 1983). Many of these images closely resemble the simulations for Scherzer-focused images, so they probably have been interpreted accurately.

In cases where packets of material several layers thick are intergrown, the simulations illustrate three important considerations. First, though a packet may contain layers with different thickness, at some focuses it may appear to contain layers with only one thickness in a 1-D HRTEM image. Second, at some focuses the packet may appear to contain a different number of layers than it actually contains. These two effects can be eliminated if the images are obtained at the Scherzer focus. Third, though a packet may contain layers with only one thickness, at some focuses it may appear to contain layers with different thicknesses. This effect can occur in Scherzer-focused images when the structure of the boundary differs on either side of the packet (e.g., a packet of lizardite). Images of mixed-layer intergrowths should be interpreted very carefully, even when proper focus is used.

Guidelines for future 1-D HRTEM of sheet silicates

On the basis of the simulations, several guidelines should be followed when studying sheet silicates with 1-D HRTEM images:

1. When possible, obtain images at more than one focus. For accurate compositional periodicities in 2:1 layer structures, obtain images with the objective lens overfocused. For accurate structural periodicities, obtain images with the objective lens underfocused to the Scherzer focus. It is especially important to set the focus accurately since apparent layer thicknesses vary with focus and some structures (for example, chlorites and some micas) exhibit image reversals with the microscope underfocused only slightly above or below the Scherzer focus.
2. Orient the crystal as accurately as possible. When the specimen is not oriented perfectly, image detail is lost and correlation between the image and structure changes. However, limited structural and compositional information often can be obtained from periodicities present in images, even when the crystal is not in perfect orientation.
3. Use an objective aperture that is matched to the electron microscope's point-to-point resolution and centered accurately around the central beam. Smaller apertures degrade image detail, producing images that often contain ambiguous information, while larger apertures can result in spurious image detail and degradation of contrast.
4. When the microscope is equipped to collect analytical data, analyze the area after HRTEM imaging.
5. Base interpretations on as many types of data possible. X-ray diffraction and analytical data offer information complementary to that from HRTEM images. However, because HRTEM studies typically address problems for which X-ray methods are unsuitable, there is no replacement for careful experimental TEM technique.
6. Avoid overinterpreting 1-D HRTEM data. Fringe thickness may not reflect layer thickness accurately, and fringe position may not correspond exactly to layer position. Estimates of an individual layer's thickness, however, can be useful for distinguishing some defect structures. Such an estimate is most accurate when it is made by measuring a region that contains both the defect and adjacent host material and then subtracting the thickness of the host.

Conclusions

One-dimensional HRTEM images of sheet silicates can provide important information. However, since the imaging conditions (focus, specimen orientation) strongly affect the images, even these simple images are best interpreted by comparing experimental images to comput-

er-simulated images. The computer-simulated images demonstrated that compositional periodicities due to one-dimensional cation ordering are best imaged with the microscope overfocused and that structural information on layer sequences is accurately imaged only with the microscope underfocused to the Scherzer focus. Slight deviations in focus can strongly affect 1-D HRTEM images and could result in incorrect image interpretations; thus, it is essential to control focus accurately. In some cases, other types of data (e.g., X-ray data, analytical data, or 1-D HRTEM images taken at several focuses from the same region) can be used to support an interpretation of an HRTEM image. However, when other data are not available, some ambiguities may be inherent in the interpretation.

Although the simulations presented here do not apply in their details to all electron microscopes, they do serve to illustrate the types of variations to be expected from simple 1-D HRTEM images of sheet silicates. We encourage others to simulate images for their specific structures and imaging conditions.

Acknowledgments

We thank K. J. T. Livi for helpful discussions on HRTEM imaging of sheet silicates; C. R. Kincaid, M. Stevens, and P. Dunn for computer assistance; M. O'Keefe for providing the SHRLI software; and A. Baronnet, M. O'Keefe, and D. Bish for providing helpful comments on the original manuscript. The work was supported by NSF grant EAR-86-09277 and Conoco, Inc.

References cited

Ahn, J.H., and Buseck, P.R. (1989) Layer-stacking sequences and structural disorder in mixed-layer illite/smectite: Image simulations and HRTEM imaging. American Mineralogist, 75, 267–275.

Ahn, J.H., and Peacor, D.R. (1985) Transmission electron microscopic study of diagenetic chlorite in Gulf Coast argillaceous sediments. Clays and Clay Minerals, 33, 228–236.

——— (1986) Transmission and analytical electron microscopy of the smectite-to-illite transition. Clays and Clay Minerals, 34, 165–179.

——— (1987a) Kaolinitization of biotite: TEM data and implications for an alteration mechanism. American Mineralogist, 72, 353–356.

——— (1987b) Transmission electron microscopic study of the diagenesis of kaolinite in Gulf Coast argillaceous sediments. In L.G. Schultz, H. van Olphen, and F.A. Mumpton, Eds., Proceedings of the International Clay Conference, Denver, 1985, p. 151–157. The Clay Minerals Society, Bloomington, Indiana.

——— (1990) Mixed-layer illite/smectite from Gulf Coast shales: A reappraisal of TEM images. Clays and Clay Minerals, in press.

Ahn, J.H., Peacor, D.R., and Coombs, D.S. (1988) Formation mechanisms of illite, chlorite and mixed-layer illite-chlorite in Triassic volcanogenic sediments from the Southland Syncline, New Zealand. Contributions to Mineralogy and Petrology, 99, 82–89.

Allpress, J.G., Hewat, E.A., Moodie, A.F., and Sanders, J.V. (1972) *n*-beam lattice images. I. Experimental and computed images from $W_4Nb_{26}O_{77}$. Acta Crystallographica, A28, 528–536.

Amouric, M., Mercuriot, G., and Baronnet, A. (1981) On computed and observed HRTEM images of perfect mica polytypes. Bulletin de Minéralogie, 104, 298–313.

Amouric, M., Gianetto, I., and Proust, D. (1988) 7, 10 and 14 Å mixed-layer phyllosilicates studied structurally by TEM in pelitic rocks of the Piemontese zone (Venezuela). Bulletin de Minéralogie, 111, 29–37.

Bailey, S.W., and Brown, B.E. (1962) Chlorite polytypism: I. Regular and semi-random one-layer structures. American Mineralogist, 47, 819–850.

Banfield, J.F., and Eggleton, R.A. (1988) Transmission electron microscope study of biotite weathering. Clays and Clay Minerals, 36, 47–60.

Cowley, J.M., and Moodie, A.F. (1957) The scattering of electrons by atoms and crystals, I. A new theoretical approach. Acta Crystallographica, 10, 609–619.

Deer, W.A., Howie, R.A., and Zussman, J. (1966) An introduction to the rock forming minerals. Longman, London.

Eggleton, R.A., and Banfield, J.F. (1985) The alteration of granitic biotite to chlorite. American Mineralogist, 70, 902–910.

Gruner, J.W. (1934) The structures of vermiculites and their collapse by dehydration. American Mineralogist, 19, 557–575.

Guthrie, G.E., Jr. (1989) Electron microscopy of fluid-mineral interactions. Ph.D. thesis, The Johns Hopkins University, Baltimore, Maryland.

Guthrie, G.D., Jr., and Veblen, D.R. (1989a) High-resolution transmission electron microscopy of mixed-layer illite/smectite: Computer simulations. Clays and Clay Minerals, 37, 1–11.

——— (1989b) High-resolution transmission electron microscopy applied to clay minerals. In L.M. Coyne, S.W.S. McKeever, and D.F. Blake, Eds., Spectroscopic characterization of minerals and their surfaces. Symposium Series 415, American Chemical Society, Washington, D.C.

Hazen, R.M., and Burnham, C.W. (1973) The crystal structures of one-layer phlogopite and annite. American Mineralogist, 58, 889–900.

Iijima, S., and Buseck, P.R. (1978) Experimental study of disordered mica structures by high-resolution electron microscopy. Acta Crystallographica, A34, 709–719.

Ilton, E.S., and Veblen, D.R. (1988) Copper inclusions in sheet silicates from porphyry Cu deposits. Nature, 334, 516–518.

Lee, J.H., Ahn, J.H., and Peacor, D.R. (1985) Textures in layered silicates: Progressive changes through diagenesis and low-temperature metamorphism. Journal of Sedimentary Petrology, 55, 532–540.

Lee, J.H., and Guggenheim, S. (1981) Single crystal X-ray refinement of pyrophyllite-1*Tc*. American Mineralogist, 66, 350–357.

Lee, J.H., and Peacor, D.R. (1985) Ordered 1:1 interstratification of illite and chlorite: A transmission and analytical electron microscopy study. Clays and Clay Minerals, 33, 463–467.

Lee, J.H., Peacor, D.R., Lewis, D.D., and Wintsch, R.P. (1986a) Chlorite-illite/muscovite interlayered and interstratified crystals: A TEM/STEM study. Contributions to Mineralogy and Petrology, 88, 372–385.

——— (1986b) Evidence for syntectonic crystallization for the mudstone to slate transition at Lehigh Gap, Pennsylvania, U.S.A. Journal of Structural Geology, 8, 767–780.

Livi, K.J.T., and Veblen, D.R. (1987) "Eastonite" from Easton, Pennsylvania: A mixture of phlogopite and a new form of serpentine. American Mineralogist, 72, 113–125.

Maresch, W.V., Massonne, H.-J., and Czank, M. (1985) Ordered and disordered chlorite/biotite interstratifications as alteration products of chlorite. Neues Jahrbuch für Mineralogie, 152, 79–100.

Mathieson, A.McL. (1958) Mg-vermiculite: A refinement and re-examination of the crystal structure of the 14.36 Å phase. American Mineralogist, 43, 216–227.

Meike, A., Wenk, H.-R., O'Keefe, M.A., and Gronsky, R. (1988) Atomic resolution microscopy of carbonates. Interpretation of contrast. Contributions to Mineralogy and Petrology, 15, 427–437.

Mellini, M. (1982) The crystal structure of lizardite *1T*: hydrogen bonds and polytypism. American Mineralogist, 67, 587–598.

Nelson, B.W., and Roy, R. (1958) Synthesis of chlorites and their structural and chemical constitution. American Mineralogist, 43, 707–725.

O'Keefe, M.A. (1973) *n*-beam lattice images. IV. Computed two-dimensional images. Acta Crystallographica, A29, 389–401.

——— (1984) Electron image simulation: A complementary processing technique. In J.J. Hren, F.A. Lenz, E. Munro, and P.B. Sewell, Eds., Electron optical systems, p. 209–220. SEM Inc., AMF O'Hare, Chicago.

O'Keefe, M.A., Buseck, P.R., and Iijima, S. (1978) Computed crystal structure images for high resolution electron microscopy. Nature, 274, 322–324.

Olives Baños, J. (1985) Biotites and chlorites as interlayered biotite-chlorite crystals. Bulletin de Minéralogie, 108, 635–641.

Olives Baños, J., and Amouric, M. (1984) Biotite chloritization by inter-

layer brucitization as seen by HRTEM. American Mineralogist, 69, 869–871.

Perdikatsis, B., and Burzlaff, H. (1981) Strukturverfeinerung am Talk $Mg_3[(OH)_2Si_4O_{10}]$. Zeitschrift für Kristallographie, 156, 177–186.

Richardson, S.M., and Richardson, J.W., Jr. (1982) Crystal structure of a pink muscovite from Archer's Post, Kenya: Implications for reverse pleochroism in dioctahedral micas. American Mineralogist, 67, 69–75.

Self, P.G., and O'Keefe, M.A. (1988) Calculation of diffraction patterns and images for fast electrons. In P.R. Buseck, J.M. Cowley, and L. Eyring, Eds., High-resolution transmission electron microscopy, p. 244–307. Oxford University Press, Oxford.

Shirozu, H., and Bailey, S.W. (1962) Chlorite polytypism: III. Crystal structure of an orthohexagonal iron chlorite. American Mineralogist, 50, 868–885.

——— (1966) Crystal structure of a two-layer Mg-vermiculite. American Mineralogist, 51, 1124–1143.

Spence, J.C.H. (1988) Experimental high-resolution electron microscopy (2nd edition). Oxford University Press, Oxford.

Spinnler, G.E., Self, P.G., Iijima, S., and Buseck, P.R. (1984) Stacking disorder in clinochlore chlorite. American Mineralogist, 69, 252–263.

Thompson, J.B., Jr. (1978) Biopyriboles and polysomatic series. American Mineralogist, 63, 239–249.

Veblen, D.R. (1983) Microstructures and mixed layering in intergrown wonesite, chlorite, talc, biotite, and kaolinite. American Mineralogist, 68, 566–580.

——— (1985) High-resolution transmission electron microscopy. In J.C. White, Ed., Applications of electron microscopy in the earth sciences, p. 63–90. Mineralogical Association of Canada, Toronto, Canada.

Veblen, D.R., and Buseck, P.R. (1979) Serpentine minerals: Intergrowths and new combination structures. Science, 206, 1398–1400.

——— (1980) Microstructures and reaction mechanisms in biopyriboles. American Mineralogist, 65, 599–623.

Veblen, D.R., and Ferry, J.M. (1983) A TEM study of the biotite-chlorite reaction and comparison with petrologic observations. American Mineralogist, 68, 1160–1168.

Veblen, D.R., Guthrie, G.D., Jr., Livi, K.J.T., and Reynolds, R.N., Jr. (1990) High-resolution transmission electron microscopy and electron diffraction of mixed-layer illite/smectite: Experimental results. Clays and Clay Minerals, 38, 1–13.

Yau, Y., Anovitz, L.M., Essene, E.J., and Peacor, D.R. (1984) Phlogopite-chlorite reaction mechanisms and physical conditions during retrograde reactions in the Marble Formation, Franklin, New Jersey. Contributions to Mineralogy and Petrology, 88, 299–306.

Manuscript received April 3, 1989
Manuscript accepted November 27, 1989